Available online at www.sciencedirect.com
SCIENCE DIRECT®
Journal of Solid State Chemistry 178 (2005) 3176–3182
JOURNAL OF SOLID STATE CHEMISTRY
www.elsevier.com/locate/jssc

$La_{2.50}K_{1.50}IrO_7$: An example of an $n = 2$ member of the $[A_nB_{n-1}O_{3n}][A'_2O]$ family of perovskite-related oxides

Samuel J. Mugavero III, Mark D. Smith, Hans-Conrad zur Loye*

Department of Chemistry and Biochemistry, University of South Carolina, Columbia, SC 29208, USA

Received 12 April 2005; received in revised form 14 June 2005; accepted 18 July 2005

Abstract

Single crystals of a new lanthanum potassium iridate, $La_{2.50}K_{1.50}IrO_7$, have been grown from a molten hydroxide flux. The structure, which is best described as resulting from the stacking of $[AO_3]$ and mixed $[A_2O]$ layers, is an $n = 2$ member of the $[A_nB_{n-1}O_{3n}][A'_2O]$ family of perovskite-related oxides. $La_{2.50}K_{1.50}IrO_7$ is comprised of $[La_2IrO_6]$ layers containing isolated $[IrO_6]$ octahedra and these layers are separated by a $[La_{0.50}K_{1.50}O]^+$ layer. The compound crystallizes in the $R\bar{3}$ space group with $a = 5.7330(2)$ Å and $c = 18.8328(9)$ Å

Keywords: Hexagonal perovskite-intergrowth; Crystal growth; Magnetic properties; Crystal structure

1. Introduction

Over the past decades, perovskites and perovskite-related oxides have been perhaps the most studied groups of oxides. Interest for this area of solid state chemistry is generated and sustained by the ever-surprising structural diversity exhibited by this family of oxides, as well as by the extensive compositional flexibility [1] that allows for the incorporation of almost any element of the periodic table into this structure type. This ever growing structural variety results from the presence of novel layer-types found in new perovskite oxides. The cubic and hexagonal perovskite structures can both be described as resulting from the stacking of close packed $[AO_3]$ layers and the subsequent filling of the generated octahedral sites by the *B*-cation. *ABC* stacking results in the cubic perovskite structure, while *AB* stacking results in the hexagonal (2H) perovskite structure. The incorporation of modified layers into the stacking sequence generates new structural variety. For example, a new family of oxides that is generated by the incorporation of $[A'_2O]$ layers into the structure and that is described by the general formula $[A_nB_{n-1}O_{3n}][A'_2O]$ was recently reported [2]. Several examples of this family of oxides have been synthesized since and include manganates: $Ln_2Ca_2MnO_7$ (Ln = La, Nd, Sm) [3], $La_2Ba_{0.8}Sr_{0.6}Ca_{1.6}Mn_2O_{10}$ [4], and $La_4Ba_{2.6}Ca_{1.4}(Mn_4Ca)O_{19}$ [5], and ruthenates: $La_{1.2}Sr_{2.44}Pt_{0.04}Ru_{0.96}O_7$ [6] and $Ba_5Ru_2O_{10}$ [7]. Investigations into this family of oxides has led to the replacement of $[A'_2O]$ with $[A'_2(O_2)]$ layers which yields the peroxide compounds, $La_2Ca_2MnO_6(O_2)$ [8], $Ba_5Ru_2O_9(O_2)$ [7], and a novel niobate $Ba_5Nb_2O_9(O_2)$ [2,7]. Our group has recently reported the synthesis and characterization of the first iridium-containing member of this family of oxides, $Ba_{3.44}K_{1.56}Ir_2O_{10}$ [9], which is isostructural with $Ba_5Ru_2O_{10}$ [7] and an $n = 3$ member of this family of oxides. In these homologues, the arrangement of the octahedra is given by the value of n, where $n = 2$ corresponds to the presence of isolated $[BO_6]$ octahedra while $n = 3$ corresponds to the presence of $[B_2O_9]$ face-sharing octahedra; these octahedra are separated from each other by the A'_2O layers.

*Corresponding author. Fax: +803 777 8508.
E-mail address: zurloye@mail.chem.sc.edu (H.-C. zur Loye).

0022-4596/$ - see front matter © 2005 Published by Elsevier Inc.
doi:10.1016/j.jssc.2005.07.031

During our studies on the single crystal growth of lanthanide-containing oxides of platinum group metals, we obtained a new perovskite-related oxide, $La_{2.50}K_{1.50}IrO_7$. To the best of our knowledge this compound is the first iridium-containing $n = 2$ member of the $[A_nB_{n-1}O_{3n}][A'_2O]$ family [10]. The crystal growth of this phase employed wet molten hydroxides, which are excellent solvents of crystallization for lanthanide-containing oxides. We have recently shown that such melts are one route for the growth of oxide single crystals containing both lanthanide and platinum group metals [11–15]. In this paper we report the crystal growth, structure determination, and magnetic characterization of $La_{2.50}K_{1.50}IrO_7$.

2. Experimental

2.1. Crystal growth of $La_{2.50}K_{1.50}IrO_7$

Single crystals of $La_{2.50}K_{1.50}IrO_7$ were grown from a high-temperature potassium hydroxide melt. La_2O_3 (Alfa Aesar 99.9%, 0.75 mmol), Ir powder (Engelhard, 99.9%, 0.5 mmol), KOH (Fisher, ACS reagent, 4.0 g) and 1.5 g of H_2O were loaded either into a silver tube that had been previously flame sealed at one end or into a silver crucible covered with a piece of silver foil. When a silver tube was used, the top of the tube was crimped and folded three times after loading before being placed upright into a programmable box furnace. The tube or crucible was heated to 650 °C in 1 h, held at that temperature for 24 h and then cooled to room temperature by shutting off the furnace. The crystals were extracted from the flux matrix by dissolving the flux in deionized water and isolating the crystals by vacuum filtration.

2.2. Scanning electron microscopy (SEM)

Crystals were analyzed by SEM using an FEI Quanta SEM instrument utilized in the low vacuum mode. Energy dispersive spectroscopy (EDS) verified the presence of lanthanum, potassium, iridium and oxygen and, within the detection limits of the instrument, confirmed the absence of extraneous elements such as silver. EDS also provided a qualitative elemental composition, where the average of the measured atomic percentages for several different crystals of $La_{2.5}K_{1.5}IrO_7$ were La (18.40%), K (10.50%), Ir (9.70%), and O (61.40%); this compares well with the calculated values of La (20.83%), K (12.50%), Ir (8.33%), and O (58.33%).

2.3. Structure determination

An irregular black crystal fragment of approximate dimensions $0.04 \times 0.04 \times 0.03\,mm^3$ was epoxied onto the end of a thin glass fiber. The data crystal was cleaved from a larger multi-domain crystal. X-ray intensity data were measured at 294(1) K on a Bruker SMART APEX CCD-based diffractometer (Mo $K\alpha$ radiation, $\lambda = 0.71073$ Å) [16]. Crystal quality and initial unit cell parameters were determined based on reflections taken from a set of three scans measured in orthogonal regions of reciprocal space. Subsequently, a full sphere of raw frame data was collected with a scan width of 0.3° in ω and an exposure time of 30 s per frame ($R_{int} = 0.0236$, ave. redundancy = 5.48, $2\theta_{max} = 65.2°$). The raw data frames were integrated with SAINT+ [16], which also applied corrections for Lorentz and polarization effects. The final unit cell parameters were determined by least-squares refinement of 1406 reflections with $I > 5\sigma(I)$ from the data set. Analysis of the data showed negligible crystal decay during data collection. Due to the lack of well-defined faces, an empirical absorption correction based on the multiple measurement of equivalent reflections was applied with the program SADABS [16]. Full-matrix least-squares refinement against F^2 and difference Fourier calculations were performed with SHELXTL [17].

$La_{2.50}K_{1.50}IrO_7$ crystallizes in the trigonal/rhombohedral system. Systematic absences in the intensity data positively ruled out a c-glide symmetry element, leaving the space groups $R3$, $R\bar{3}$, $R3m$, $R\bar{3}m$ and $R32$ as candidates. The space group choice is not unambiguous, with reasonable solutions obtainable in any of the five. After trial refinements in each space group, the best solution was judged to be in $R\bar{3}$. This space group preserves the highest symmetry with minimal oxygen disorder. There are five atomic positions in $R\bar{3}$ (Table 2). Ir1 and La1 refine normally. The La2 site displays an enlarged displacement parameter when fixed at 100% lanthanum. Refinement of the La2 site occupation factor (sof) resulted in a significant decrease from unity. This was ascribed to La/K site mixing for consistency with elemental content (EDS/SEM) results. Refinement of this site as a mixed La/K site constrained to full occupancy resulted in the ratio 0.252(5)/0.748(5) (La2/K2). Common displacement parameters and z-coordinates were refined for both atoms of this site. Refinement of the sofs for Ir1 and La1 yielded 0.994(4) and 1.005(4), respectively, and these sofs were therefore fixed at full occupancy. Oxygen O2 is disordered in a similar manner as previously observed (3,6–7). O2 is disordered about a site of $\bar{3}$ symmetry (0, 0, $\frac{1}{2}$) in $R\bar{3}$, generating six equivalent positions. Free refinement of the O2 sof gave 0.15(1) and was subsequently fixed at $\frac{1}{6}$. The longest distance between oxygen atoms in the O2 disorder assembly is 1.38(5) Å. This distance is far shorter than

the typical peroxide $(O_2)^{2-}$ distance (ca. 1.55–1.62 Å) found in similar oxides. The O2–O2 bond length together with the refined occupancy leads us to conclude that an isolated, disordered oxide ion O^{2-} exists on this site. All atoms were successfully refined with anisotropic displacement parameters with the exception of O2. Anisotropic refinement of O2 yielded a strongly oblate ellipsoid, indicating this atom is probably disordered over even more than the six equivalent positions generated. O2 was refined isotropically for the final cycles. Anisotropic displacement plots of Ir1, La1, and La2/K2 are shown in Fig. 1. The crystal was refined as a merohedral twin emulating the $\bar{3}m$ Laue group with the twin matrix (by rows) [010/100/00$\bar{1}$], yielding a major twin fraction of 0.502(9). At convergence the residual electron density extremes were $+1.96$ and $-2.19\,e\,Å^{-3}$, located 0.61 and 1.15 Å from La1, respectively. The final refined crystallographic composition is $La_{2.504(5)}K_{1.496(5)}IrO_7$.

Refinement was also performed in $R\bar{3}m$, $R3m$, $R32$ and $R3$. Refinement in $R\bar{3}m$ yielded good refinement statistics and normal behavior of the metal atoms; however, the O1 displacement parameter refined as unusually elongated and required a split position model with O1 disordered across a mirror plane. The disorder of O1 implies two rotational orientations of the IrO_6 octahedron. Examination of the difference map calculated in the absence of O1 supported this model, showing two electron density peaks of roughly equal magnitude in the O1 region. In addition, the six-fold disorder of the O2 site persists. Similar disorder of O1 and O2 was also observed in $R3m$. Refinement in $R32$ or $R3$ results in an ordered IrO_6 octahedron and three-fold disorder of O2. The necessity of invoking IrO_6 (O1) disorder in the higher space groups and the perseverance of the O2 disorder along with the greater number of refinement parameters required in these lower space groups leads us to conclude that the best description of the $La_{2.5}K_{1.5}IrO_7$ structure is as a merohedral twin in the centrosymmetric $R\bar{3}$ space group. Table 1 lists a summary of crystallographic data and refinement statistics; Tables 2–4 list the atomic coordinates with equivalent isotropic displacement parameters, anisotropic displacement parameter values and selected interatomic distances, respectively.

2.4. Magnetic susceptibility

Magnetic susceptibility measurements were performed on ground single crystals of $La_{2.50}K_{1.50}IrO_7$ using a Quantum Design MPMS XL SQUID magnetometer. The sample was measured under both zero field cooled (ZFC) and field cooled (FC) conditions in applied fields of 1 and 10 kG over the temperature range of $2\,K \leqslant T \leqslant 300\,K$. The sample was contained in a gel capsule suspended in a plastic straw for immersion

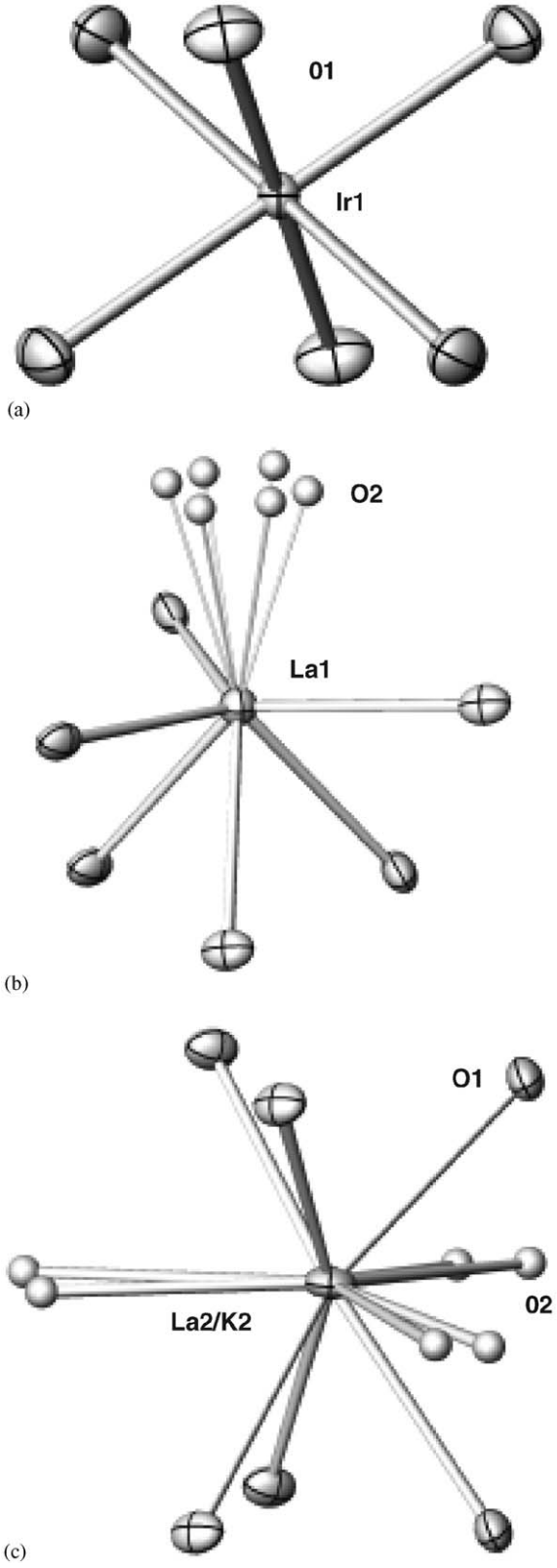

Fig. 1. Anisotropic displacement parameter plots of the coordination environments of Ir1, La1, and La2/K2. (a) Ir1 is in an octahedral coordination environment, (b) La1 is in a pseudo-seven-fold coordination environment and (c) La2/K2 are in a capped-trigonal prismatic coordination environment. The displacement ellipsoids are drawn at the 50% probability level.

into the SQUID. The small diamagnetic contribution of the gelatin capsule containing the sample had negligible contribution to the overall magnetization, which was dominated by the sample. The sample used for the magnetic measurements was analyzed by powder X-ray diffraction. A Rietveld refinement on this very small sample demonstrated that, within the limits of powder X-ray diffraction, the sample was phase pure $La_{2.50}K_{1.50}IrO_7$. The plot of the Rietveld refinement can be found in the supplementary materials.

Table 1
Crystal data and structural refinement of $La_{2.50}K_{1.50}IrO_7$

Empirical formula	$La_{2.504(5)}K_{1.496(5)}IrO_7$
Formula weight ($g\,mol^{-1}$)	710.46
Space group	$R\bar{3}$
Unit cell dimensions	
a (Å)	5.7330(2)
c (Å)	18.833(1)
V (Å^3)	536.05(4)
Z	3
Density (calculated) ($g\,cm^{-3}$)	6.602
Absorption coefficient (mm^{-1})	34.066
$F(000)$	912
Crystal size (mm)	$0.04 \times 0.04 \times 0.03$
θ_{max} (deg)	32.59
Index ranges	$-8 \leqslant h \leqslant 8$; $-8 \leqslant k \leqslant 7$; $-28 \leqslant l \leqslant 28$
Reflections collected	2427
Independent reflections	443 [R(int) = 0.0236]
No. parameters refined, restraints	25, 0
R indices (all data)	$R_1(F) = 0.0234$, $wR_2(F^2) = 0.0501$
Goodness-of-fit on F^2	1.160
Residual e^- density max. peak/ max. hole (e^- Å^{-3})	1.962/−2.185

3. Results and discussion

3.1. Crystal structure

Single crystals of $La_{2.50}K_{1.50}IrO_7$ were grown in a sealed silver tube or a covered silver crucible containing a molten potassium hydroxide solution, which has proved to be an excellent medium for synthesizing lanthanide-containing oxides [18] due to their acid–base properties that are best described by the Lux–Flood acid–base definition [19,20]. Since the tube or crucible was sealed or covered, the dehydration of the melt was slowed significantly and, hence, a relative constant acidity of the melt was maintained over the course of the experiment. As the water content of the tube greatly affects yield and phase purity, it represents an important experimental variable that must be controlled. In order to obtain essentially phase pure batches of

Table 4
Selected interatomic distances (Å) for $La_{2.50}K_{1.50}IrO_7$

$La_{2.50}K_{1.50}IrO_7$	
Ir(1)–O(1) × 6	1.966(5)
La(1)−O(1) × 3	2.503(6)
La(1)−O(1) × 3	2.630(5)
La(1)−O(2) × 3 (× 1/6)	2.33(5)
La(1)−O(2) × 3 (× 1/6)	2.40(5)
La(2)/K(2)−O(1) × 3	2.599(5)
La(2)/K(2)–O(1) × 3	2.737(5)
La(2)/K(2)–O(2) × 3 (× 1/6)	2.66(3)
La(2)/K(2)–O(2) × 3 (× 1/6)	2.86(5)
O(2)−O(2)	1.38(5)

Table 2
Atomic coordinates and equivalent isotropic displacement parameters for $La_{2.50}K_{1.50}IrO_7$, respectively

Atom	Site	Occupancy	x	y	z	U_{eq}
Ir(1)	3a	1	0	0	0	0.0092(1)
La(1)	6c	1	0	0	0.37994(3)	0.0155(2)
La(2)/K(2)	6c	0.252(5)/0.748(5)	0	0	0.17388(6)	0.0195(4)
O(1)	18f	1	0.3218(10)	0.0960(11)	0.0576(3)	0.020(1)
O(2)	18f	1/6	0.099(9)	0.134(6)	0.502(3)	$U_{iso} = 0.025(6)$

U_{eq} is defined as one-third of the trace of the orthogonalized U_{ij} tensor.

Table 3
Anisotropic displacement parameters U_{ij} (Å^2) for $La_{2.50}K_{1.50}IrO_7$

Atom	U_{11}	U_{22}	U_{33}	U_{12}	U_{13}	U_{23}
Ir(1)	0.008(1)	0.008(1)	0.011(1)	0	0	0.004(1)
La(1)	0.015(1)	0.015(1)	0.017(1)	0	0	0.007(1)
La(2)/K(2)	0.024(1)	0.024(1)	0.010(1)	0	0	0.012(1)
O(1)	0.013(2)	0.026(3)	0.017(2)	0.001(2)	−0.003(2)	0.007(2)

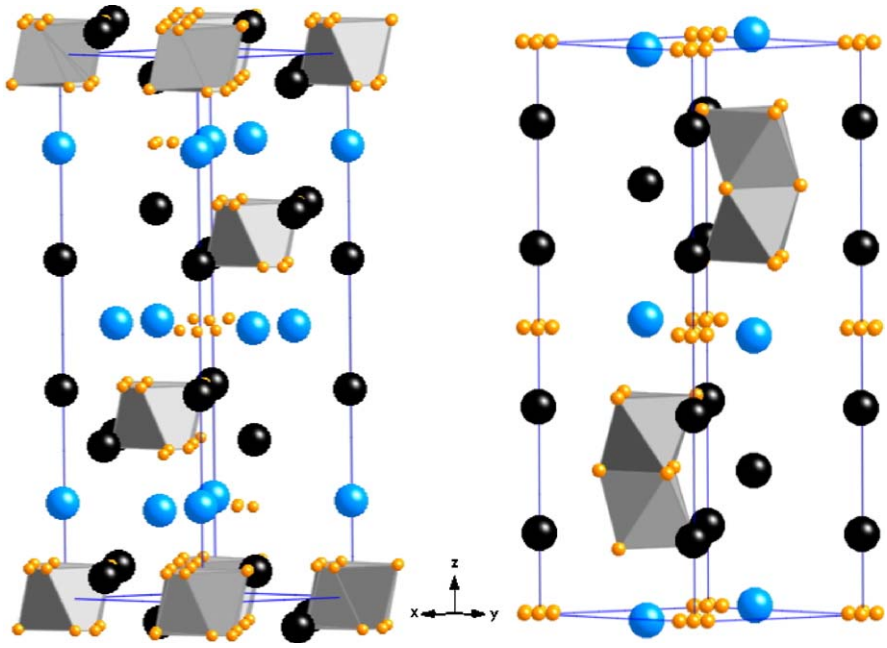

Fig. 2. The crystal structures of $n = 2$ member, $La_{2.5}K_{1.5}IrO_7$ (left) and $n = 3$ member, $Ba_{3.44}K_{1.56}Ir_2O_{10}$ (right). In the $La_{2.5}K_{1.5}IrO_7$ structure, the gray polyhedra are IrO_6 octahedra, the black spheres are lanthanum atoms, the blue spheres are the La2/K2 atoms, and the orange spheres are oxygen atoms. In $Ba_{3.44}K_{1.56}Ir_2O_{10}$, the gray polyhedra are Ir_2O_9 face-shared octahedra dimers, the black spheres are barium atoms, the blue spheres are the Ba3/K1 atoms, and the orange spheres are oxygen atoms.

$La_{2.50}K_{1.50}IrO_7$ crystals, the water content had to be high (an additional 1.5 mL H_2O per tube vs. a more typical 1.0 mL H_2O per tube). Impurities were relatively easy to separate because they consisted of either tan La_2O_3 crystals or pieces of silver from the tube or crucible.

The single crystal structure of $La_{2.50}K_{1.50}IrO_7$ was refined in the space group $R\bar{3}$. The compound is isostructural with $La_2Ca_2MnO_7$ and $La_{1.2}Sr_{2.4}Pt_{0.04}Ru_{0.96}O_7$, which are $n = 2$ members of the $[A_nB_{n-1}O_{3n}][A'_2O]$ family of structures consisting of close-packed $[AO_3]$ and $[A'_2O]$ layers. A representation of the crystal structure is shown in Fig. 2. The structure consists of $[La_2IrO_6]^-$ anionic layers that contain isolated lanthanum atoms in a pseudo-seven-fold coordination environment and isolated IrO_6 octahedra. The Ir–O bond distance of 1.969(6) Å is consistent with the expected values of iridium(V) in an octahedral coordination environment. These layers are charge compensated by cationic $[La_{0.50}K_{1.50}O]^+$ layers that contain mixed occupancy (La2/K2) capped trigonal prismatic sites to yield an overall charge neutral structure containing iridium in the +5 oxidation state. The source of potassium was the reactive potassium hydroxide flux. For comparison, the iridium containing $n = 3$ member of this family of oxides, $Ba_{3.44}K_{1.56}Ir_2O_{10}$, is depicted next to the $La_{2.50}K_{1.50}IrO_7$ structure in Fig. 2. Both structures have A'_2O layers, $[La_{0.50}K_{1.50}O]^+$ and $[Ba_{0.44}K_{1.56}O]^+$, respectively, and in both structures site mixing is observed only in this layer. The $[La_2IrO_6]^-$ and $[Ba_3Ir_2O_9]^-$ layers, respectively, contain the isolated $[IrO_6]$ octahedra and $[Ir_2O_9]$ face-sharing octahedra dimers and have full site occupancy. The oxidation states, in both cases, are quite high and based on the crystallographic refinements, Ir is +5.00 and +5.78 in $La_{2.50}K_{1.50}IrO_7$ and $Ba_{3.44}K_{1.56}Ir_2O_{10}$, respectively. The possibility of the O2 atoms in $La_{2.5}K_{1.5}IrO_7$ belonging to a peroxide unit (O_2^{2-}) as exhibited in $La_2Ca_2MnO_6(O_2)$ (8), $Ba_5Ru_2O_9(O_2)$ (7), and $Ba_5Nb_2O_9(O_2)$ (2,7) can be ruled out by the short O2–O2 distance of 1.38(5) Å, compared to the O2–O2 distances in the peroxide units of the above compounds of 1.624, 1.554, and 1.619 Å, respectively.

3.2. Magnetism

The FC temperature dependence of the magnetic susceptibility for $La_{2.50}K_{1.50}IrO_7$ at 1 kG is shown in Fig. 3. The susceptibility increases with decreasing temperature over the entire measured temperature range and the ZFC and FC data overlay in all cases. It is known that Ir(V) has a nonmagnetic ground state and therefore contributes very little to the overall susceptibility [21–24]. We can determine the magnetization at zero temperature following the procedure of Hayashi et al. [22] by plotting the squared magnetic moment as a function of temperature. From a linear fit extrapolation of this plot to zero temperature, it is possible to calculate the Ir(IV) content in this compound that could arise from an oxygen deficiency. The μ^2 vs. T plot, shown as

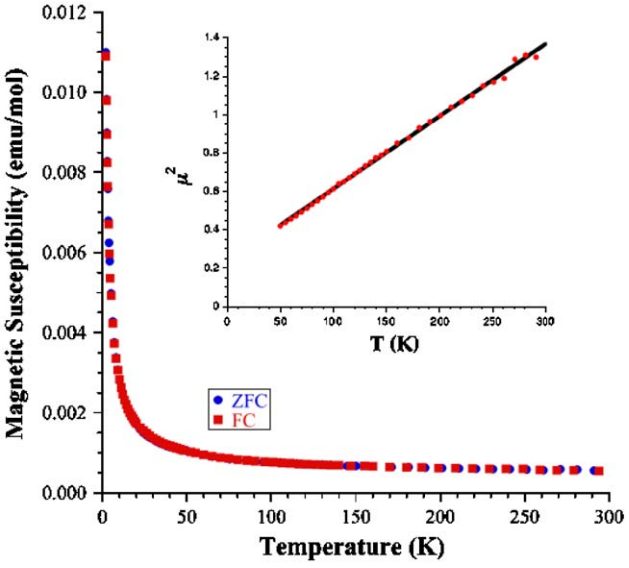

Fig. 3. Temperature dependence of the zero field cooled (blue circles) and field cooled (red squares) magnetic susceptibility of $La_{2.5}K_{1.5}IrO_7$. Inset: temperature dependence of the squared magnetic moment of $La_{2.5}K_{1.5}IrO_7$. A linear fit of the data is shown as a solid line.

the inset in Fig. 3, corresponds to an Ir(IV) (d^5, $s = \frac{1}{2}$) content of approximately 7%. This is higher than expected based on the ideal structure composition of $La_{2.50}K_{1.50}IrO_7$, which indicates that the compound contains iridium in the pentavalent oxidation state. We have, however, noted that Ir(V)-containing oxide crystals are unstable to prolonged exposure to moisture, which suggests that the Ir(IV) present in this sample may be due to post-synthesis sample degradation, rather than to incomplete oxidation of iridium during synthesis.

4. Conclusion

The use of a molten potassium hydroxide flux has enabled us to synthesize a new $n = 2$ member of the $[A_nB_{n-1}O_{3n}][A'_2O]$ family of hexagonal intergrowth perovskite-related oxides, $La_{2.50}K_{1.50}IrO_7$. This is the second example of an iridium-containing oxide in this family and also the first example of an $n = 2$ iridate. Magnetic susceptibility measurements are indicative of a paramagnetic compound and by plotting μ^2 vs. T, we were able to determine the oxidation state of iridium in $La_{2.50}K_{1.50}IrO_7$.

5. Supplementary materials

A Rietveld refinement of the sample used for magnetic measurements is included. Further details of the crystal structure investigations can be obtained from the Fachinformationszentrum Karlsruhe, 76344 Eggenstein-Leopoldshafen, Germany, (fax 49) 7247 808 666; email: crystdata@fiz.karlsruhe.ed) on quoting the depository number CSD-415292.

Acknowledgments

This work was supported by the Department of Energy through grant DE-FG02-04ER46122 and the National Science Foundation through grant DMR: 0134156 and DMR:0450103.

Appendix A. Supplementary materials

Supplementary data associated with this article can be found in the online version at doi:10.1016/j.jssc.2005.07.031.

References

[1] E. Stitzer, J. Darriet, H.-C. zur Loye, Curr. Opin. Solid State Mater. Sci. 5 (2001) 535.
[2] F. Grasset, C. Dusserrat, J. Darriet, J. Mater. Chem. 7 (1997) 1911.
[3] Y.-X. Wang, L.-J. Bie, Y. Du, J.-H. Lin, C.-K. Loong, J.W. Richardson Jr., L.-P. You, J. Solid State Chem. 177 (2004) 65.
[4] L. Bie, J. Lin, Y. Wang, C.-K. Loong, Inorg. Chem. Commun. 5 (2002) 966.
[5] L. Bie, Y. Wang, J. Lin, C.-K. Loong, J.W. Richardson Jr., L. You, C. Dong, Chem. Mater. 15 (2003) 516.
[6] S.G. Ebbinghaus, J. Solid State Chem. 177 (2004) 817.
[7] F. Grasset, M. Zakhour, J. Darriet, J. Alloy Compd. 287 (1999) 25.
[8] E. Gaudin, G. Goglio, A. Besnard, J. Darriet, J. Solid State Chem. 175 (2003) 124.
[9] S.-J. Kim, M.D. Smith, J. Darriet, H.-C. zur Loye, J. Solid State Chem. 177 (2004) 1493.
[10] S.J. Mugavero III, M.D. Smith, H.-C. zur Loye, in: Proceedings of the 55th Southeast Regional Meeting of the American Chemical Society 415, American Chemical Society, Atlanta, GA, 2003. AN 2004:137731. Since then another report of an $n = 2$ iridate has appeared: http://de.arxiv.org/abs/cond-mat/0504171.
[11] M.J. Davis, S.J. Mugavero III, K.I. Glab, M.D. Smith, H.-C. zur Loye, Solid State Sci. 6 (2004) 413.
[12] M.J. Davis, M.D. Smith, K.E. Stitzer, H.-C. zur Loye, J. Alloy Compd. 351 (2003) 95.
[13] W.R. Gemmill, M.D. Smith, H.-C. zur Loye, Inorg. Chem. 43 (2004) 4254.
[14] W.R. Gemmill, M.D. Smith, H.-C. zur Loye, J. Solid State Chem. 177 (2004) 3560.
[15] S.J. Mugavero III, M.D. Smith, H.-C. zur Loye, J. Solid State Chem. 178 (2005) 200.
[16] SAINT+ Version 6.22 and SADABS 6.22 Bruker Analytical X-ray Systems SMART Version 5.625, Bruker Analytical X-ray Systems Inc., Madison, WI, 1998.
[17] G.M. Sheldrick, SHELXTL Version 5.1, Bruker Analytical X-ray Systems, Inc., Madison, WI, 1997.

[18] S.W. Keller, V.A. Carlson, D. Sanford, F. Stenzel, A.M. Stacy, G.H. Kwei, M. Alario-Franco, J. Am. Chem. Soc. 116 (1994) 8070.
[19] H. Lux, *Z.* Elektrochem. 45 (1939) 303.
[20] H. Flood, T. Forland, Acta Chem. Scand. 1 (1947) 592.
[21] M. Walewski, B. Buffat, G. Demazeau, F. Wagner, M. Pouchard, P. Hagenmuller, Mater. Res. Bull. 18 (1983) 881.
[22] K. Hayashi, G. Demazeau, M. Pouchard, P. Hagenmuller, Mater. Res. Bull. 15 (1980) 461.
[23] A.V. Powell, J.G. Gore, P.D. Battle, J. Alloy Compd. 201 (1993) 73.
[24] M.J. Davis, S.J. Mugavero III, K.I. Glab, M.D. Smith, H.-C. zur Loye, Solid State Sci. 6 (2004) 413.